https://doi.org/10.5194/tc-2023-68
Preprint. Discussion started: 8 May 2023

The Cryosphere Discussions

Modeling the timing of Patagonian Ice Sheet retreat in the Chilean Lake District from 23-10 ka

Joshua Cuzzone[1], Matias Romero[2], Shaun A. Marcott[2]

[1]Joint Institute for Regional Earth System Science and Engineering, University of California, Los Angeles
[2]Department of Geoscience, University of Wisconsin, Madison

Correspondence to: Joshua K. Cuzzone (Joshua.K.Cuzzone@jpl.nasa.gov)

Abstract

Studying the retreat of the Patagonian Ice Sheet (PIS) during the last deglaciation represents an important opportunity to understand how ice sheets outside the polar regions have responded to deglacial changes in temperature and large-scale atmospheric circulation. At the northernmost extension of the PIS during the last glacial maximum (LGM), the Chilean Lake District (CLD) was influenced by the southern westerly winds (SWW), which strongly modulated the hydrologic and heat budget of the region. Despite progress in constraining the nature and timing of deglacial ice retreat across this area, considerable uncertainty in the glacial history still exists due to a lack of geologic constraints on past ice margin change. Where the glacial chronology is lacking, ice sheet models can provide important insight into our understanding of the characteristics and drivers of deglacial ice retreat. Here we apply the Ice Sheet and Sea-level System Model (ISSM) to simulate the LGM and last deglacial ice history of the PIS across the CLD at high spatial resolution (450 meters). We present an ensemble of LGM ice sheet model experiments using climate inputs from the Paleoclimate Modelling Intercomparison Project (PMIP4) and a transient simulation of ice margin change across the last deglaciation using climate inputs from the CCSM3 Trace-21ka experiment. We find that although the simulated LGM temperature is primarily responsible for differences in simulated ice geometries, wintertime precipitation also plays an important role in modulating LGM ice sheet volume and extent. The simulated deglaciation is found to match existing geologic constraints that indicate widespread ice margin retreat between 18 to 16.5 ka. Following this interval our simulations suggest that the ice sheet retreated rapidly, and by 15 ka onward, only mountain glaciers remained across the CLD in contrast with sparse geologic data that indicate a local ice cap remaining until 10ka. Additionally, our results suggest that modest variations in winter precipitation (~10%) can modulate the pacing of ice retreat by 1-2 ka, which has implications when comparing simulated outputs of ice margin change to geologic reconstructions. Therefore, these LGM and deglacial experiments signify the importance in constraining the deglacial strength, latitudinal position, and extent of the SWW and its influence on the hydrologic and heat budget and also highlight the importance in constraining paleoclimate parameters critical to modelling and understanding the drivers of deglacial PIS behavior.

https://doi.org/10.5194/tc-2023-68
Preprint. Discussion started: 8 May 2023

The Cryosphere Discussions
Open Access

1 Introduction

During the Last glacial maximum (LGM), the Patagonian Ice Sheet (PIS) covered an area along the Andes mountains from 38°S to 55°S, with an estimated sea-level equivalent ice volume of 1.5 meters (Davies et al., 2020). At the northernmost extent of the PIS, across an area presently known as the Chilean Lake District (CLD), the LGM to deglacial ice behavior and related climate forcings has been a subject of historical interest (Mercer, 1972; Porter, 1981; Lowell et al., 1995; Andersen et al, 1999; Denton et al., 1999; Glasser et al., 2008, Moreno et al., 2015; Kilian and Lamy, 2012; Lamy et al., 2010; 2015), and have served as important constraints towards understanding the drivers of ice sheet change across centennial to millennial timescales. Currently, PATICE (Davies et al., 2020) serves as the latest and most complete reconstruction of the entire PIS during the last glacial and last deglaciation. Across the CLD (Figure 1), the LGM ice limits are well constrained by terminal moraines in the southwest and western margins (Denton et al., 1999; Glasser et al.,

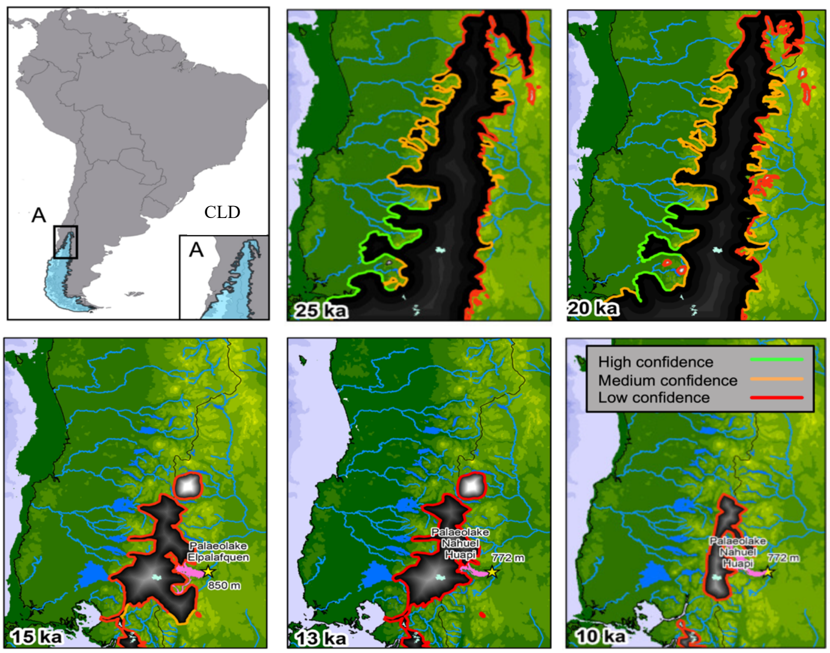

Figure 1. Location of the study area across the Chilean Lake District (CLD; Upper Left Panel). The reconstructed ice extent from PATICE for the PIS across the CLD at 25 ka, 20 ka, 15 ka, 13 ka, and 10 ka are taken from Davies et al., 2020. The color of the line marking the reconstructed ice extent corresponds to the confidence in the reconstruction as described in section 3.3.

2008, Moreno et al., 2015). However, due to a lack of geomorphological and geochronologic constraints on past ice margin change, the reconstructed deglaciation remains highly uncertain.

While deglacial warming is a primary driver of ice retreat across the CLD, evidence suggests that variations in precipitation patterns influenced the timing and magnitude of this retreat (Moreno et al., 1999; Rojas et al., 2009). The wintertime climate across South America is strongly

https://doi.org/10.5194/tc-2023-68
Preprint. Discussion started: 8 May 2023

influenced by the southern westerly winds (SWW), which exert a large control on the synoptic scale hydrologic and heat budget (Garreaud et al., 2013). During the LGM and last deglaciation, the position, strength, and extent of the SWW varied latitudinally, altering overall ice sheet mass balance (Mercer, 1972; Denton et al., 1999; Lamy et al., 2010; Kilian and Lamy, 2012; Boex et al., 2013). Terrestrial paleoclimate proxies indicate that the CLD was strongly influenced by a shifting SWW position during the last deglaciation (Moreno et al., 2015; Moreno and Videla, 2016). However, due to limitations in the spatial abundance and resolution of these paleoclimate proxies (Kohfeld et al., 2013), as well as certainty in deglacial ice sheet reconstructions (see Figure 1), assessment of the climatic drivers of past ice sheet change across this region remains difficult.

Early paleo ice sheet modelling experiments across the PIS have focused on evaluating the relationship between the simulated LGM ice sheet geometry in response to spatially uniform temperature change (Hulton et al., 2002; Sugden et al., 2002; Hubbard et al., 2005). While these early simulations provided constraints on PIS areal extent, ice volume, and sensitivity to LGM temperature depressions, spatially varying temperature and precipitation were not considered. Recently, Yan et al. (2022) simulated the PIS behavior at the LGM using an ensemble of climate model output from the Paleoclimate Modelling Intercomparison Project (PMIP4; Kageyama et al., 2021). Results best matching the empirical reconstructions from PATICE (Davies et al., 2020) suggest that reduction in temperature was likely the main driver of PIS LGM extent, although the authors found that variation in regional LGM climate can have large impacts on the simulated ice sheet geometry. This evidence is supported by recent glacier modelling across the northeastern Patagonian Andes which suggests that increases in precipitation during the termination of the LGM are necessary to achieve modeled fit with reconstructed glacier extent (Muir et al., 2023; Leger et al., 2021). Additionally, Martin et al. (2022) found that precipitation greater than present day are needed to explain late glacial and Holocene ice readvance of the Monte San Lorenzo ice cap, lying to the southeast of the current Northern Patagonian Ice Field. These regional studies therefore provide further evidence that late glacial and deglacial variability in the SWW influenced PIS retreat and readvance over numerous timescales.

To advance our understanding of last glacial and deglacial ice behavior across the CLD, we use the Ice Sheet and Sea-level System Model (ISSM; Larour et al., 2012) to first simulate the LGM ice geometry forced by an ensemble of climate boundary conditions from PMIP4 models (Kageyama et al., 2021). Second, we simulate the deglacial evolution of the PIS across the CLD using transiently evolving boundary conditions from a climate model simulation of the last 21,000 years (TraCE-21ka; Liu et al., 2009; He et al., 2013) which simulates large scale variability in the strength and position of the SWW (Jiang and Yan, 2020). Because there is a lack of transiently evolving ice sheet model simulations of the PIS across the last deglaciation, our aim is to provide possible constraints on the nature of ice retreat across the CLD region, from which the reconstructions (PATICE; Davies et al., 2020) are uncertain. Also, by assessing the sensitivity of our ice sheet experiments to a range of climatic boundary conditions, we aim to provide additional insight into the dominant climatic controls on the deglacial evolution of the PIS in the CLD region.

2 Methods: Model description and setup

2.1 Ice sheet model

https://doi.org/10.5194/tc-2023-68
Preprint. Discussion started: 8 May 2023

In order to simulate the ice margin migration across the CLD during the LGM and last deglaciation, we use the Ice Sheet and Sea-level System Model (ISSM), a thermomechanical finite-element ice sheet model (Larour et al., 2012). Because of the high topographic relief across the CLD and associated impact on ice flow, we use a higher-order approximation to solve the momentum balance equations (Dias dos Santos et al., 2022). This ice flow approximation is a depth-integrated formulation of the higher-order approximation of Blatter (1995) and Pattyn (2003), which allows for an improved representation of ice flow compared with more traditional approaches in paleo-ice flow modelling (e.g., Shallow Ice Approximation or hybrid approaches; Hubbard et al., 2005; Leger et al., 2022; Yan et al., 2022), while allowing for reasonable computational efficiency. Our model domain comprises the northernmost LGM extent of the PIS across the CLD, extending beyond the LGM ice extent reconstructed from Davies et al. (2020) and ends along the northern extent of the Golfo de Ancud (Figure 2).

We rely on anisotropic mesh adaptation to create a non-uniform model mesh that varies based upon gradients in bedrock topography from the General Bathymetric Chart of the Oceans (GEBCO; GEBCO Bathymetric Compilation Group, 2021), a terrain model for ocean and land.

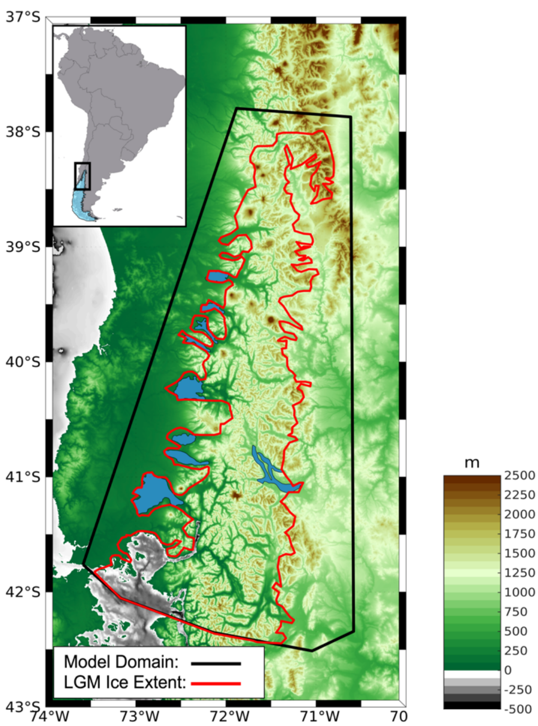

Figure 2. Bedrock topography for our study area (meters). Our model domain (shown as the black line), encompasses the reconstructed LGM ice limit (shown in red) from PATICE (Davies et al., 2020). Present day lakes are shown in blue.

For the land component, the GEBCO model uses version 2.2 of the Surface Radar Topography Mission data (SRTM15_plus; Tozer et al., 2019), to create a 15 arc second gridded output of terrain

https://doi.org/10.5194/tc-2023-68
Preprint. Discussion started: 8 May 2023

The Cryosphere Discussions
Open Access EGU

elevation relative to sea level. Our ice sheet model horizontal mesh resolution varies from 3 km in areas of low bedrock relief to 450 meters in areas where gradients in the bedrock topography is high and comprises of 40,000 model elements.

Although evidence suggests that while southernmost glaciers across the PIS may have been polythermal, data suggests that the majority of the PIS was temperate (isothermal). Accordingly, recent ice flow modelling (Leger et al., 2021) suggests that varying ice viscosity mainly impacts the accumulation zone thickness in simulations of paleoglaciers in Northeastern Patagonia, with minimal impacts on overall glacier length and extent. Therefore, our model is 2-dimensional and we do not solve for ice temperature and viscosity allowing for increased computational efficiency. For our purposes, we use Glen's flow law (Glen, 1955) and set the ice viscosity following the rate factors in Cuffey and Paterson (2010) assuming an ice temperature of -0.2°C. We use a linear friction law (Budd et al., 1979)

$$\tau_b = -k^2 N v_b \tag{1}$$

where τ_b represents the basal stress, N represents the effective pressure, and v_b is the magnitude of the basal velocity. The spatially varying friction coefficient, k, is constructed following Åkesson et al. (2018):

$$k = 200 \times \frac{\min[\max(0, z_b + 600), z_b]}{\max(z_b)} \tag{2}$$

where z_b is the height of the bedrock with respect to sea level. Using this parameterization, basal friction is larger across high topographic relief and lower across valleys, and areas below sea level.

Currently ISSM is undergoing model developments to include a full treatment of solid earth-ice and sea-level feedbacks (Adhikari et a., 2016). Therefore, at this time, there is no interaction between our simulated ice sheet and the solid earth. We do however account for changes in the geoid at the LGM and across the last deglaciation using a time dependent forcing from Caron et al. (2018) that accounts for relative sea-level changes following setups in Briner et al. (2020) and Cuzzone et al. (2019).

2.2 Experimental Design

We perform simulations of a.) the LGM configuration for the PIS across our model domain, and b.) a transient simulation across the last deglaciation.

LGM simulations: We simulate the LGM configuration of the PIS across our model domain using climate model output from the Paleoclimate Model Intercomparison Project (PMIP4; Kageyama et. al., 2021) as well as climate model output at the LGM and through the last deglaciation from a transient climate model simulation (Liu et al., 2009; He et al., 2013). Monthly mean output of temperature and precipitation at varying horizontal resolution (Table 1) are used from these simulations as inputs to our glaciological model (full climate forcings details are further described in section 2.4).

https://doi.org/10.5194/tc-2023-68
Preprint. Discussion started: 8 May 2023

Table 1. List of model output used for the climate boundary conditions and the corresponding spatial resolution.

Model	Spatial Resolution	Reference
CCSM4 (TraCE-21ka)	3.75° x 3.75°	Liu et al. (2009) He et al. (2013)
MPI-ESM1.2 (MPI)	1.8° x 1.8°	Mauritsen et al. (2019)
MIROC-ES2L (MIROC)	2.8° x 2.8°	Ohgaito et al. (2021) Hajima et al. (2020)
IPSLCM5A2 (IPSL)	3.8° x 1.9°	Sepulchre et al. (2020)
AWIESM2 (AWI)	1.8° x 1.8°	Sidorenko et al. (2019)

Simulation across the last deglaciation: In order to simulate the ice history across the last deglaciation we use monthly climate model output from the National Center for Atmospheric Research Community Climate System Model (CCSM3) TraCE-21ka transient climate simulation of the last deglaciation (Liu et al., 2009; He et al., 2013). We use the monthly mean output every 50 years across the last deglaciation.

2.3 Surface Mass Balance

In order to simulate the deglaciation of the PIS across our model domain we require inputs of temperature and precipitation to estimate the surface mass balance. To derive snow and ice melt we use a positive degree day model (Tarasov and Peltier, 1999; Le Morzadec et al., 2015; Cuzzone et al., 2019; Briner et al., 2020). Our degree day factor for snow melt is 3 mm $^{\circ}C^{-1}day^{-1}$ and 6 mm $^{\circ}C^{-1}day^{-1}$ for bare ice melt, and we use a lapse rate of 6 ºC to adjust the temperature of the climate forcings to surface elevation. These values are typical of those used to model contemporary and paleo glaciers across Patagonia (see Fernandez et al., 2016 Table 3; Yan et al., 2022).

2.4 Climate forcings

In order to scale monthly temperature and precipitation across the LGM and last deglaciation we applied a commonly used modeling approach (Pollard et al., 2012; Cuzzone et al., 2022; equations 3 and 4). First, we use the monthly mean climatology of temperature and precipitation for the period 1979-2018 ($\bar{T}_{(1979-2018)}, \bar{P}_{(1979-2018)}$) from the Center for Climate Resilience Research Meteorological dataset version 2.0 (CR2MET; Boisier et al., 2018). This output, which uses information from a climate reanalysis and is calibrated against rain-gauge observations, is provided at 5 km spatial resolution. We then bilinearly interpolate these fields onto our model mesh.

$$T_t = \bar{T}_{(1979-2018)} + \Delta T_t \tag{3}$$

$$P_t = \bar{P}_{(1979-2018)} + \Delta P_t \tag{4}$$

Next, anomalies of the monthly temperature and precipitation fields are computed as the difference from each model's preindustrial control run and interpolated onto our model mesh (ΔT_t and ΔP_t). Therefore, LGM anomalies for each model are computed as well as anomalies across the last deglaciation (Liu et al., 2009; He et al., 2013). These anomalies are added to the contemporary

https://doi.org/10.5194/tc-2023-68
Preprint. Discussion started: 8 May 2023

monthly mean as shown in equations 3 and 4, to produce the monthly temperature and precipitation fields at LGM and across the last deglaciation (T_t and P_t).

2.5 Ice front migration and iceberg calving

Across most of our domain, there is evidence for an advance of piedmont glaciers across glacial outwash during the LGM, which formed the physical boundary for some of the existing terminal moraines around the lakes within the CLD (Bentley, 1996; Bentley, 1997). Where there were proglacial lakes along the westward ice front in the CLD, evidence suggests that ice was grounded during the LGM (Lago Puyehue; Heirman et al., 2011). During deglaciation, iceberg calving into the proglacial lakes may have occurred (Davies et al., 2020), with evidence suggesting that local topography and calving may have controlled the spatially irregular timing of abandonment from the terminal moraines surrounding the proglacial lakes (Bentley, 1997). However, because inclusion of ice-lake interactions is relatively novel for numerical ice flow modeling (Sutherland et al., 2020; Quiquet et al., 2021; Hinck et al., 2022), we choose to not model the evolution and influence of proglacial lakes on the deglaciation across this model domain. Instead, we only simulate calving where the PIS interacts with the ocean.

We track the motion of the ice front using the level-set method described in Bondzio et al. (2016; equation 3) in which the ice velocity (v_f) is a function of the ice velocity vector at the ice front (v), the calving rate (c), the melting rate at the calving front ($\dot{M}$), and where n is the unit normal vector pointing horizontally outward from the calving front. For these simulations the melting rate is assumed to be negligible compared to the calving rate, so $\dot{M}$ is set to 0.

$$v_f = v - (c + \dot{M})\, n \qquad (5)$$

To simulate calving we employ the more physically based Von Mises stress calving approach (Morlighem et al., 2016) which relates the calving rate (c) to the tensile stresses simulated with the ice, where $\tilde{\sigma}$ is the von Mises tensile strength, $\|v\|$ is the magnitude of the horizontal ice velocity, and σ_{max} is the maximum stress threshold which has separate values for grounded and floating ice.

$$c = \|v\| \frac{\tilde{\sigma}}{\sigma_{max}} \qquad (6)$$

The ice front will retreat if von Mises tensile strength exceeds a user defined stress threshold, which we set to 200 kPa for floating ice and 1 MPa for grounded ice. This calving law has been applied in Greenland to assess marine terminating icefront stability (Bondzio et al., 2016; Morlighem et al., 2016; Choi et al., 2021; Cuzzone et al., 2022) and for our simulations applies where ocean is present such as the Seno de Reloncaví and the Golfo de Ancud (see Figure 2).

3 Results

3.1 LGM Experiments

https://doi.org/10.5194/tc-2023-68
Preprint. Discussion started: 8 May 2023

The Cryosphere
Discussions
Open Access
EGU

In order to arrive at a steady state LGM ice geometry, we first initialize our model with an ice-free configuration. The constant LGM monthly climatology of temperature and precipitation are then applied, as well as the prescribed LGM geoid from Caron et al. (2018). We allow the ice sheet to relax for 10,000 years, during which, the ice sheet is free to grow and expand until it reaches a steady state ice geometry and volume, in equilibrium with the climate forcings. These relaxation steps are performed for the separate experiments using the individual climate model output described in section 2.2.

3.1.1 LGM climate

Shown in Figures 3 are the anomalies (LGM-preindustrial) of summer temperature (DJF) and winter precipitation (JJA) for each climate model. The area averaged anomaly is shown in the upper lefthand corner of each sub figure. In general, the climate models simulate an LGM climate that is colder than preindustrial, with summer temperature anomalies ranging between -4.7°C (TraCE-21ka) to -7.9°C (MPI). Generally, the climate models exhibit larger cooling during the LGM compared to the preindustrial over the central to southern portions of our model domain, although the magnitude of those changes differ amongst the individual models with the AWI and MPI models exhibiting the strongest cooling.

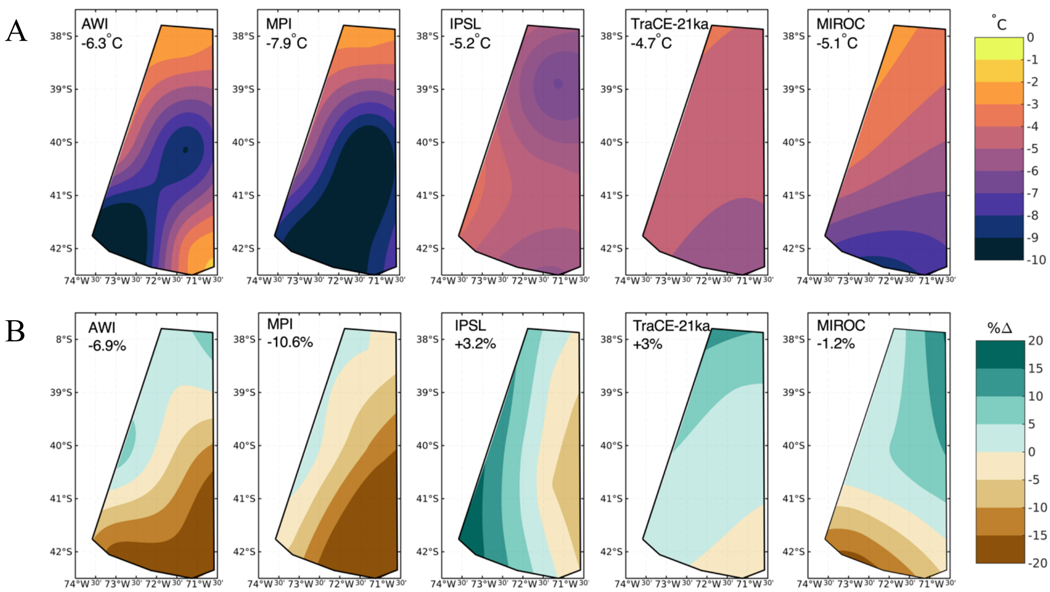

Figure 3. A). Anomalies of summer temperature (DJF; top panels) and, B). winter precipitation (JJA; bottom panels) for each climate model. Anomalies are taken as the difference between the LGM and preindustrial (LGM-PI), with the precipitation anomalies expressed as the percent difference of the LGM from preindustrial. The area averaged value of the anomaly is shown for each model in the upper left of each panel.

The differences in the winter precipitation anomalies are quite large both in magnitude and spatial variability. Some models (AWI, MPI, and MIROC) simulate drier winter conditions across our model domain during the LGM compared to the preindustrial, while IPSL and TraCE-21ka models simulate wetter conditions. While there is considerable spread in the gradient of the precipitation anomalies, most models tend to have drier LGM conditions towards the southern boundary of the

https://doi.org/10.5194/tc-2023-68
Preprint. Discussion started: 8 May 2023

model domain with the exception of the IPSL model, which has a west to east gradient in the precipitation anomaly.

The spatial resolution of the temperature and precipitation anomalies is also evident. Models with a higher spatial resolution (AWI and MPI; see table 1) simulate a tighter gradient in temperature and precipitation, and therefore the range between the minimum and maximum anomalies are greatest for these models. Conversely, the more coarse climate model output of TraCE-21ka depicts more spatially consistent anomalies.

3.1.2 LGM Ice Geometry

In Figure 4, the simulated LGM ice thickness is shown for each individual simulation, with the red outline indicating the reconstructed LGM (20 ka) ice extent from PATICE (Davies et al., 2020). Across our model domain, bedrock elevation increases from west to east, with deep valleys interspersed across most of our model domain (Figure 2). Consistent across all simulations, ice thickness is greatest in these valleys (upwards of 2000 meters) where driving stresses dominate

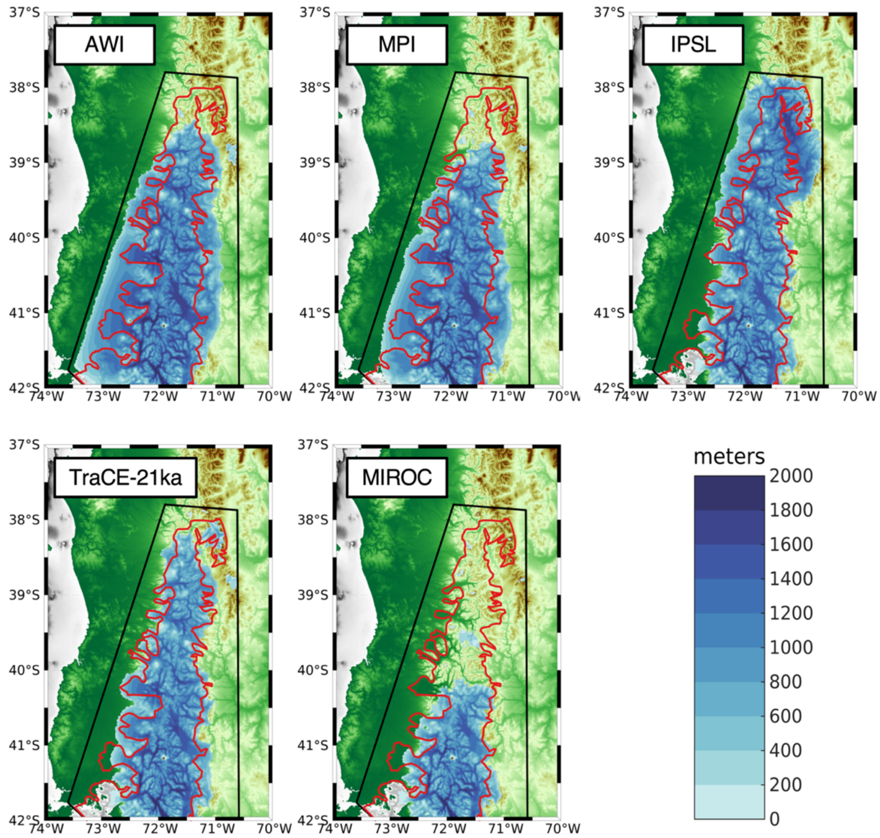

Figure 4. The simulated LGM ice thickness (meters) is shown for each experiment using the different climate boundary conditions. The black outline denotes our ice sheet model boundary, and the red line denotes the LGM reconstructed ice extent from PATICE (Davies et al., 2020).

https://doi.org/10.5194/tc-2023-68
Preprint. Discussion started: 8 May 2023

and where bedrock geometry controls the flow of ice from higher terrain and through these valleys (Figure 5). Ice thickness generally thins towards the ice margins, but is thick in many of the fast-flowing outlets along the margin that drain the ice sheet interior (Figure 5). Across the highest terrain such as the many volcanoes across the CLD, ice is comparatively thinner than the surrounding valleys. Despite the differences in ice sheet configurations, all simulations reach an LGM state that is defined by a north-south ice divide with east and west flowing ice reaching velocities upwards of 1 km/yr and greater (Figure 5).

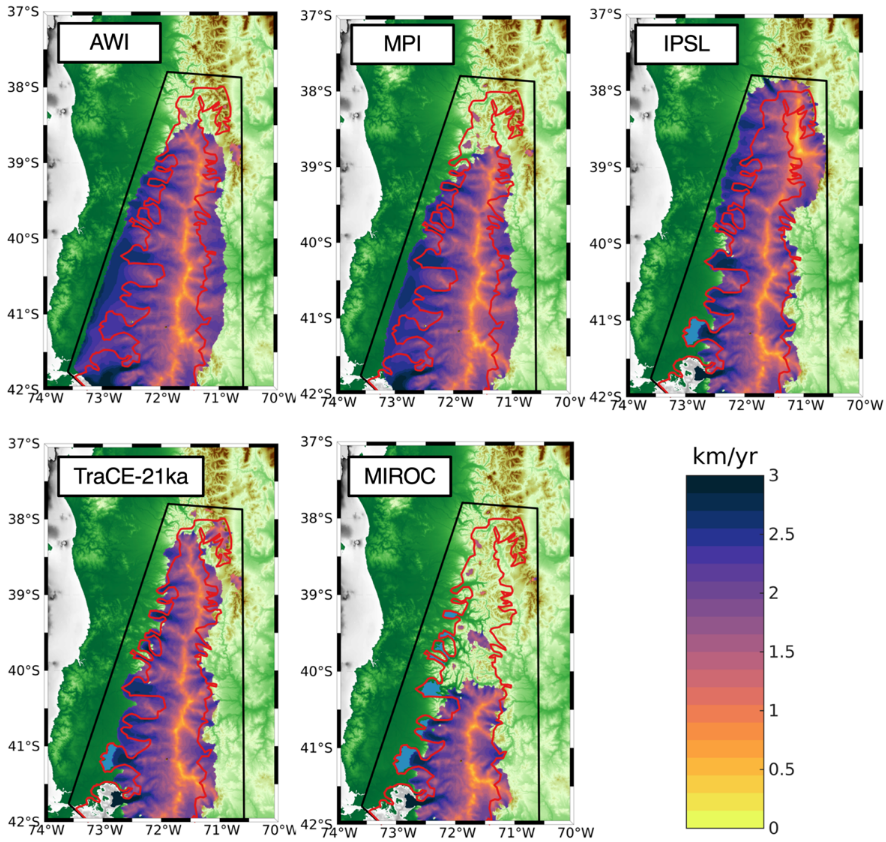

Figure 5. The simulated LGM ice surface velocity (km/yr) is shown for each experiment using the different climate boundary conditions. The black outline denotes our ice sheet model boundary, and the red line denotes the LGM reconstructed ice extent from PATICE (Davies et al., 2020).

Generally, all simulations exhibit ice cover across the southern portion of the model domain, while the simulations using the AWI and MPI LGM climatologies having more extensive ice cover especially along the western margin, extending outward of the reconstructed LGM ice extent from PATICE (Davies et al., 2020). This is consistent with the greater magnitude in simulated summertime cooling at the LGM along the south and southwestern boundary of our model domain for the AWI and MPI models despite reduced wintertime precipitation (Figure 3). Along the southern portion of the model domain, simulations using the IPSL, TraCE-21ka, and MIROC

https://doi.org/10.5194/tc-2023-68
Preprint. Discussion started: 8 May 2023

climate fail to simulate ice cover across the present-day Seno de Reloncaví and the Golfo de Ancud, consistent with lower summertime cooling across this region in comparison to the AWI and MPI models (Figure 3A). Across the northernmost portion of the model domain, the simulation using the MIROC climatology, which simulates the least LGM cooling across this area (Figure 3A), produces no ice cover. Only the simulations using the IPSL and TraCE-21ka climatology produce ice cover that matches well within the PATICE (Davies et al., 2020) reconstructed boundary.

3.1.3 LGM ice extent and sensitivity to climate

The resulting ice volume across our model domain is plotted against the LGM anomaly of summer temperature and winter precipitation in Figure 6. Model simulations that fall closer to the lower left have cooler summer LGM temperature anomalies and drier winter precipitation anomalies relative to the other climate models used in this study. Simulations that fall in the upper right of Figure 6 have less LGM summertime cooling, but higher wintertime precipitation anomalies

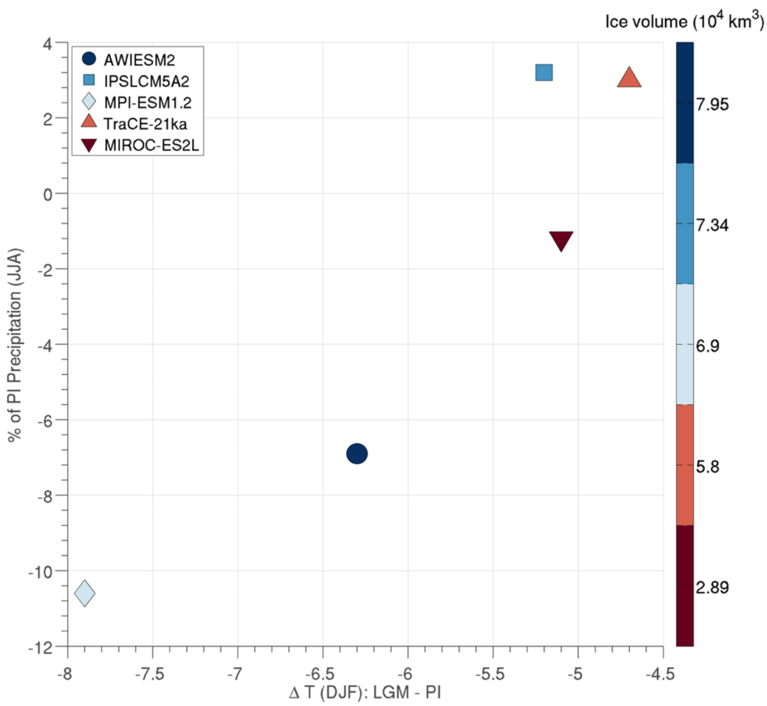

Figure 6. The simulated LGM ice volume (km^3) is color coded for each individual model, with darker reds corresponding to lower ice volume and darker blue corresponding to higher ice volume. This is plotted against the wintertime (JJA) precipitation anomaly expressed as the percent difference between the LGM and preindustrial period, and the summertime (DJF) temperature anomaly expressed as the difference between the LGM and preindustrial period.

relative to the other models used in this study. The simulated LGM ice volume is also plotted on this graph, and color coded by the climate model output used in the ice sheet simulation. For

https://doi.org/10.5194/tc-2023-68
Preprint. Discussion started: 8 May 2023

example, the experiment using the MIROC climate simulates the lowest LGM ice volume (dark red: 2.89×10^4 km^3) and the simulation using the AWI climate simulates the largest LGM ice volume (dark blue: 7.96×10^4 km^3).

For the simulation with the largest LGM ice volume (AWI climate), the area averaged LGM temperature anomaly is -6.3°C and precipitation is -6.8% relative to preindustrial. The experiment using the IPSL climate simulates the second largest ice volume and has an LGM temperature anomaly that is 1.1°C (-5.2°C) warmer than the AWI model (-6.3°C). However, of the climate models used, the IPSL model has the highest simulated increase in LGM precipitation relative to the preindustrial (+3.2%). Conversely, whereas the MPI model simulates the coldest LGM temperature anomalies (-7.9°C), it also simulates the driest climate relative to preindustrial (-10.6%), resulting in a simulated LGM ice volume that is lower than experiments using the AWI and IPSL climate.

Despite the TraCE-21ka model having a similar magnitude of precipitation increase during the LGM (+3%) compared to the IPSL model (+3.2%), it simulates less LGM cooling (-4.7°C) in comparison to IPSL (-5.2°C). This results in a 21% greater simulated ice volume for the experiment using the IPSL climate in comparison to TraCE-21ka. Lastly, the experiment using the MIROC climate model output simulates the lowest ice volume. While LGM temperature anomalies for the MIROC model (-5.2°C) are nearly identical in to the IPSL model (-5.2°C), the simulated LGM climate is overall drier (-1.2% for MIROC; +3.2% for IPSL). We note that the spatial variation in the temperature and precipitation anomalies seem to play a role in the low simulated ice volume for the experiment using the MIROC climate model output. In Figure 3a, we see that the MIROC model simulates colder and drier conditions in the south and warmer and wetter conditions across the north. These conditions are more favorable for reduced snow accumulation and negative surface mass balance across the northern portion of the model domain, leading to a lack of simulated LGM ice cover across this region (Figure 4).

3.2 Simulation of the Last Deglaciation

Monthly mean temperature and precipitation, taken every 50 years from the TraCE-21ka (Liu et al., 2009; He et al., 2013) experiment is used to drive our simulation of ice history across the last deglaciation (22 ka – 10 ka). The transient simulation is initialized with the LGM ice sheet geometry shown in Figure 4 (TraCE-21ka), and is run forward with the appropriate climate boundary conditions until 10 ka.

3.2.1 Pattern of Deglaciation

From the resulting transient simulation, we calculate the timing of deglaciation across our model domain (Figure 7A). Because of possible readvances during the deglaciation, we select the youngest age at which grid points become ice free. Our map of the simulated deglaciation can be paired with a timeseries of the rate of ice mass change (Figure 8, bottom panel) to highlight some key features in the magnitude and timing of ice retreat between 22 ka and 10 ka.

https://doi.org/10.5194/tc-2023-68
Preprint. Discussion started: 8 May 2023

The Cryosphere
Discussions
Open Access

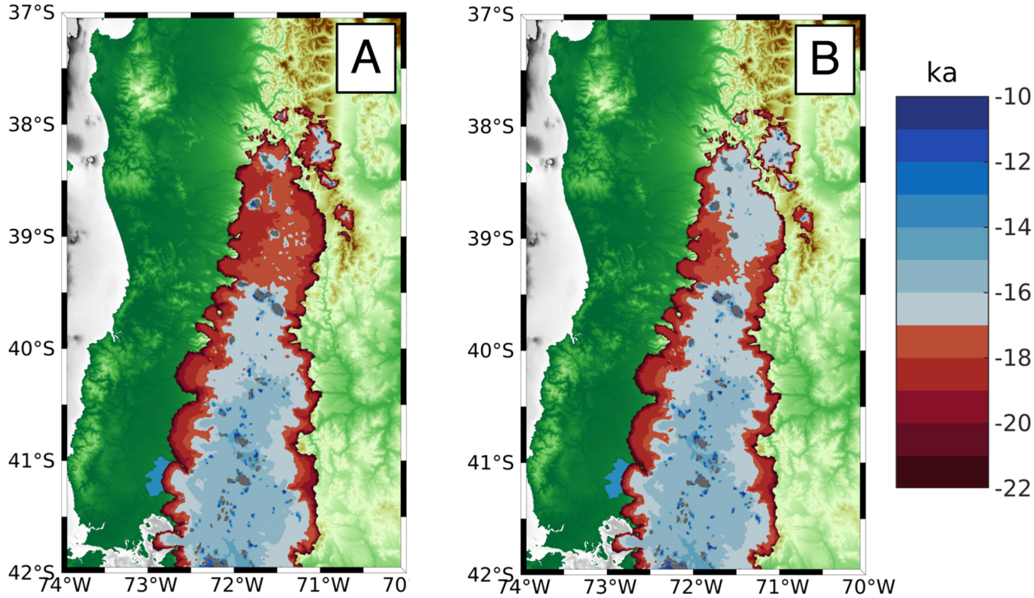

Figure 7. The simulated deglaciation age for the transient simulation from the LGM to 10 ka, for experiments where temperature and precipitation vary throughout the deglaciation based on climate boundary conditions from TraCE-21ka (A); and where precipitation is held fixed at LGM conditions but temperature varies based on climate boundary conditions from TraCE-21ka (B).

Between 22 ka to 19 ka, the ice sheet undergoes periods of minor to moderate ice mass loss and gain (Figure 8), in an interval of time where summer temperature anomalies and the corresponding ice margin remain relatively stable (Figure 7a). Between 19 ka and 18.5 ka, coincident with a rise in summertime temperature (Figure 8), a pulse of ice mass loss occurs and exceeds 5,000 GT/century before trending toward minimal ice mass loss around 18 ka as the rise in summer temperature levels off. During this time interval, the ice margin pulls back considerably towards higher terrain across the northern portion of the model domain (Figure 7A), and many of the fast-flowing outlet glaciers on the western margin retreat back towards the ice sheet interior. Between 18 ka to 16.2 ka, summer temperature rises steadily ~1.2°C and is punctuated with an abrupt warming of ~0.5°C at 16 ka (Figure 8). During this interval, ice mass loss remains high and steady at ~1000 GT/century with pulses of increased mass loss at 17.8 ka, 16.8 ka, and 16 ka varying between 2000-5000 GT/century (Figure 8).

By 17 ka, the northern portion of the model domain (north of 39.5°S), has generally become ice free for the exception of the highest terrain (e.g., mountain glaciers). By 16 ka, and between 39.5°S and 40.5°S, ice remains only on the highest terrain (Figure 7A), however ice cover persists south of 40.5°S. Between 16 ka and 15 ka, summer temperature rises ~0.5°C (Figure 8) and the remaining ice sheet retreats south of 40.5°S. By 15 ka, there is no evidence of an ice sheet, with only mountain glaciers existing across the high terrain throughout the model domain (Figure 7A).

https://doi.org/10.5194/tc-2023-68
Preprint. Discussion started: 8 May 2023

After 15 ka, TraCE-21ka simulates a short and abrupt Antarctic Cold Reversal (ACR) between 14.6 ka and 14 ka (Figure 8), before temperatures continue to rise into the early Holocene. There is only a minor ice mass gain (e.g., <500 GT/yr) during the ACR, and minimal fluctuation in ice mass after 14 ka. By 10 ka, only small mountain glaciers persist across the high terrain and volcanoes of the CLD (gray color in Figure 7).

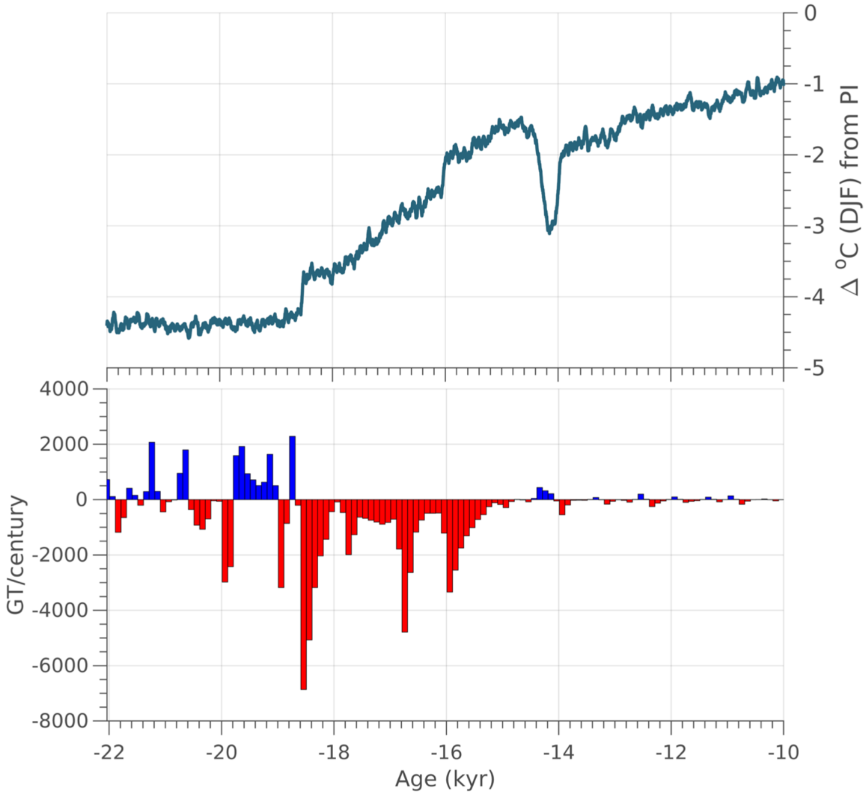

Figure 8. Top Panel: The TraCE-21ka Summer (DJF) temperature anomaly taken as the difference from the preindustrial period, area averaged across our model domain. Bottom Panel: The simulated ice mass change calculated in GT/century across the last deglaciation (22 ka to 10 ka). Red indicates ice mass loss, and blue indicates ice mass gain.

3.2.2 Sensitivity Test

The Trace-21ka model simulates upwards of 10-15% higher wintertime precipitation across the northern portion of our model domain during the LGM compared to preindustrial (Figure 3B, see TraCE-21ka). North of 40°S, wintertime precipitation is generally higher than the preindustrial until ~17.2 ka (Figure 9). Given the simulated increase in wintertime precipitation during the early deglacial (~22ka – 18ka; Figure 9) across the northern portion of the model domain, we run a sensitivity test to determine how this positive anomaly influences the simulated deglaciation. For

https://doi.org/10.5194/tc-2023-68
Preprint. Discussion started: 8 May 2023

The Cryosphere Discussions
Open Access
EGU

this test we hold the monthly precipitation constant to the mean over the interval 22 ka to 20 ka, but allow temperature to vary through the deglaciation.

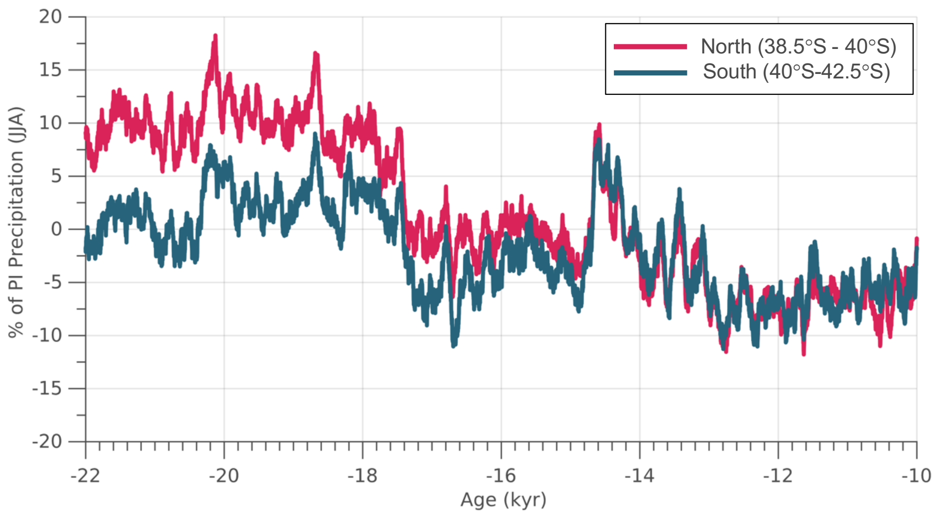

Figure 9. The winter (JJA) precipitation anomaly expressed as the percent difference from the preindustrial period. The area averaged anomaly is shown for the region north of 40°S and for the region south of 40°S (see Figure 2 for reference to the latitudinal range of our model domain).

For this experiment, it is clear that North of 40.5°S the simulated deglaciation is delayed for experiment that keeps monthly precipitation constant at the 22-20 ka mean (Figure 7B). Deglaciation is delayed upwards of 1-2 kyr's across this region in comparison to the simulation allowing precipitation to vary (Figure 7A), with the largest delay occurring across the highest terrain (e.g., northeastern portion of model domain).

3.3 Comparison to the reconstructed deglacial ice extent

Shown in Figure 1, PATICE assigns high to medium confidence to the reconstructed LGM (25 ka – 20 ka) ice extent along most of the western ice margin and portions of the eastern margin, with low confidence assigned to the northernmost ice extent. The majority of the ice history is poorly constrained (low confidence) during the deglaciation, and PATICE reconstructs a small cap that persists across the southern CLD until 10 ka, after which the ice disappears and only the Cerro Tronador glacier remains (see Figure 13 from Davies et al., 2020).

We show the simulated and reconstructed ice extent (Figure 10) as well as the calculated ice area from PATICE at 20 ka, 15 ka, and 13ka and for our transient simulation (Figure 11). Overall, the simulated ice margin and area is stable between 22 ka and 18.3 ka (Figure 11). At 22 ka (Figure 10), our model simulates a generally greater ice extent along the eastern and western margin,

https://doi.org/10.5194/tc-2023-68
Preprint. Discussion started: 8 May 2023

The Cryosphere
Discussions
Open Access
EGU

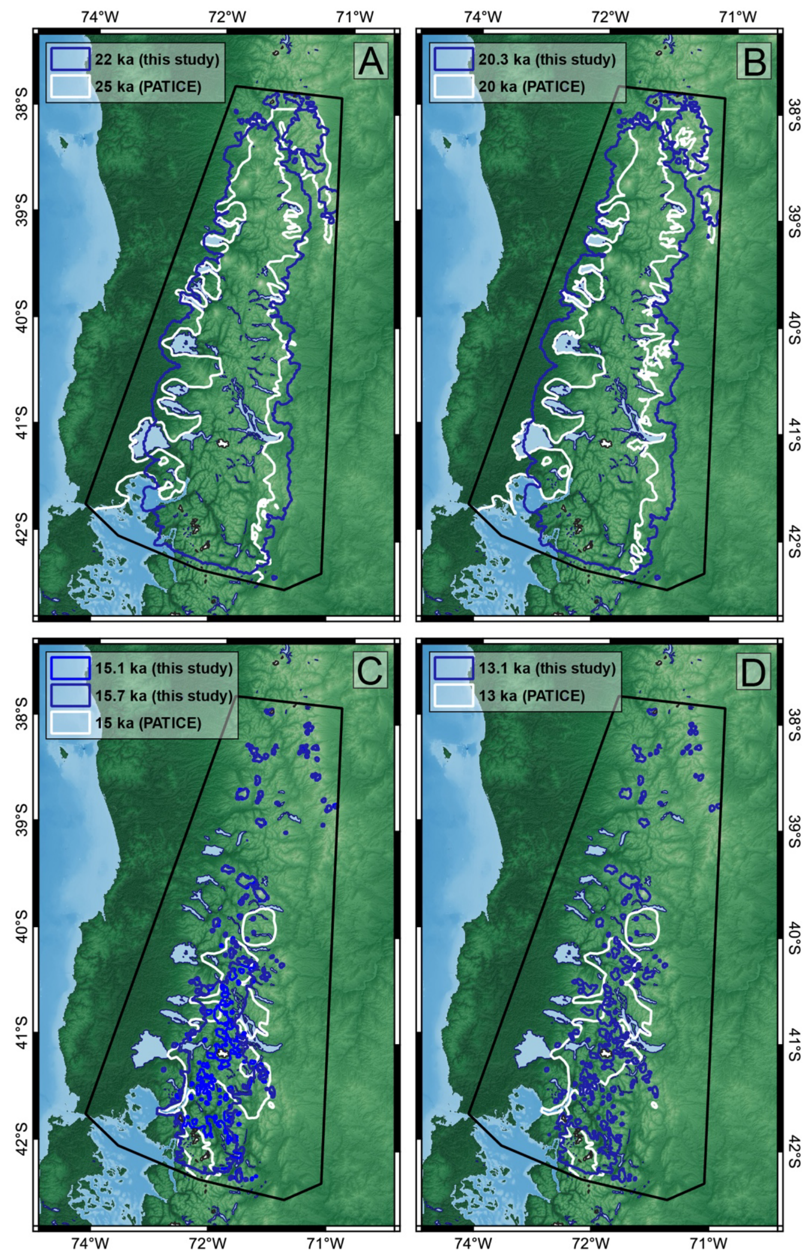

Figure 10. Comparison between the simulated ice extent at time intervals closest to the corresponding reconstructed ice extent from PATICE (Davies et al., 2020).

except at the Seno de Reloncaví, Golfo de Ancud, and Lago Llanquihue, where the simulated ice margin does not advance to the well dated terminal LGM moraines (Mercer, 1972; Porter, 1981; Andersen et al., 1999; Denton et al., 1999). At 20 ka, the simulated ice area is 4.1×10^4 km^2 which

https://doi.org/10.5194/tc-2023-68
Preprint. Discussion started: 8 May 2023

is nearly identical to the PATICE areal extent across our model domain (Figure 11). The ice margin at the Seno de Reloncaví, Lago Llanquihue, and other locations along the eastern boundary in the CLD advances slightly at 20 ka, but still remain inboard of the PATICE reconstruction for these regions. Between 18.3 ka and 15 ka large scale ice retreat occurs, and the simulated ice sheet loses 90% of its ice area (Figure 11). At 15 ka, PATICE reconstructs an existing ice cap that separates from the remainder of the PIS to the south (Figure 10). This is in contrast to the simulated ice extent, which shows that by 15 ka, the PIS across our model domain has completely retreated and only mountain glaciers exist amongst the high terrain. However, if we compare the PATICE area at 15 ka and the simulated ice area at 15.7 ka (Figure 11), they are nearly identical at 1.2×10^4 km^2. While the PATICE ice extent at 15 ka and the simulated ice extent 15.7 ka do not match completely, the simulated ice extent at 15.7 ka still has evidence of an ice cap similar to the PATICE reconstruction. Therefore, the simulated transition from ice sheet to ice cap and to discrete mountain glaciers occurs between 15.7 ka and 15 ka in our simulations. By 13 ka, our simulated ice area is 60% lower than the PATICE reconstructed area (Figure 11), and our model simulates discrete mountain glaciers while PATICE reconstructs an ice cap existing through 10 ka (Figure 10; also see Figure 1).

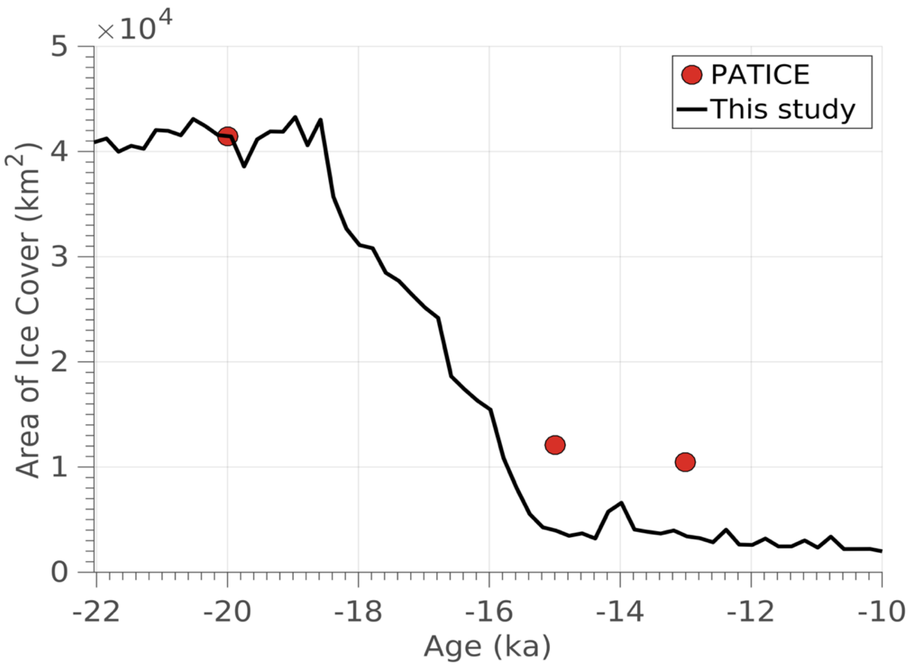

Figure 11. The simulated ice area (km^2) from 22 ka to 10 ka shown as the black line. The red dots indicate the calculated ice area across our model domain for the reconstructed ice extent from PATICE (Davies et al., 2020).

4 Discussion

4.1 Climate-ice sensitivity

https://doi.org/10.5194/tc-2023-68
Preprint. Discussion started: 8 May 2023

Determining the influence of the SWW on the heat and hydrologic budget across South America during the LGM and last deglaciation remains elusive, as limitations in paleo-proxy data and disagreement between climate models prohibit certainty (Kohfeld, 2013; Berman et al., 2018). And while evidence does suggest wetter conditions across the CLD during the late glacial (Moreno and Videla, 2016), linking the paleoclimate change in SWW position and strength from regional paleoclimate proxies remains problematic (Kohfeld et al., 2013).

The scale at which we deduce ice history and climate interactions is also important. Looking at the PIS as a whole, recent numerical ice sheet modelling studies indicate that the simulated ice extent and volume for the entire PIS at the LGM is largely controlled by the magnitude of the temperature anomaly compared to present day (Yan et al., 2022). However, regional scale ice flow modelling informed by geologic constraints on past ice margin extent show that higher precipitation during the LGM (Leger et al., 2021), the late glacial, and the Holocene (Muir et al., 2023; Martin et al., 2022) is needed to support model-data agreement. It appears that during the LGM a northward shift in the SWW (Kohfeld et al., 2013; Rojas et al., 2009; Togweillier et al., 2006) or a strengthening or expansion of the wind belt (Lamy et al., 2010) is perhaps the most likely scenario, with high frequency variability possible during the deglaciation as atmospheric reorganization altered the heat and hydrologic budget as recorded by glacier and ice sheet change (Davies et al., 2020; Boex et al., 2013).

Although our experimental setup cannot identify a clear relationship between the influence of temperature and precipitation on the simulated ice volume, these results indicate that the relationship is not simple. While the LGM cooling largely controls ice volume, wintertime precipitation, which comprises the majority of annual snow accumulation, can enhance or dampen the ice volume response to LGM temperature depressions (Figure 6). Using a small sample of LGM PMIP4 climate model output, we arrive at different simulated LGM states for the PIS across the CLD. If temperature were the primary control on ice volume, we would expect simulations using the coldest LGM climate model output to produce the highest LGM ice volumes (Figure 6). However, there are situations where this is not the case, as those simulations with higher precipitation produce higher ice volume despite modest LGM temperature depressions (i.e., Figure 6; IPSL). We note that the climate models with the coldest simulated LGM climate (AWI and MPI, Figure 3), correspondingly simulate the driest wintertime climate. Likewise models with higher spatial resolution, simulate a higher gradient in the simulated temperature and precipitation patterns. With discrepancy amongst climate model output, and a lack of paleo proxy data to constrain those models, these results illustrate that the relationship between LGM ice volume and extent across the CLD to climate is not simple as already suggested through prior work (Leger et al., 2021; Martin et al., 2022; Yan et al., 2022).

Our sensitivity test (section 3.2.2) indicates that increases (~10%) in wintertime precipitation relative to preindustrial can offset ice loss driven by deglacial warming. In our case (Figure 7A, B), deglaciation is delayed across the northern portion of the model domain upwards of 1-2 kyr. Therefore, these results show that even modest changes in wintertime precipitation can modulate the pacing and magnitude of ice retreat driven by deglacial warming on scales that are recorded in the geologic record of ice margin migration, which has large implications for model-data comparisons seeking to evaluate the impact of deglacial climate change on past ice margin migration in this region.

https://doi.org/10.5194/tc-2023-68
Preprint. Discussion started: 8 May 2023

4.2 Ice retreat across the Last Deglaciation

The PATICE dataset (Davies et al., 2020) serves as the best available reconstruction of ice margin change for the PIS across the last deglaciation. Because geochronological constraints on past PIS change are limited, the PATICE reconstruction assigns qualitative confidence to its reconstructed ice margins. Where there is agreement between geochronological and geomorphological (i.e., moraines) indicators of past ice margin history, high confidence is assigned. Where geomorphological evidence suggests the existence of past ice margins, but lacks a geochronological constraint, medium confidence is assigned. Lastly, low confidence is assigned where there is a lack of any indicators of past ice sheet extent. Across the CLD, the LGM ice extent is well constrained by geologic proxies particularly in the west and southwest (Figure 1). The moraines that constrain the piedmont ice lobes that formed along the western boundary and are now presently lakes have reasonable age control (Denton et al., 1999; Moreno et al., 1999; Lowell et al., 1995) and give confidence to the LGM ice margin limits. Beyond this region, age control is sparse along the western boundary for the timing of LGM ice extent, but the existence of well-defined moraines along lakes in the northern CLD are assumed to be in sync with those moraines deposited to the south (Denton et al., 1999). Low confidence remains in the geologic reconstruction of the LGM ice boundary along the eastern margin. In general, deglaciation from the maximum LGM ice extent begins between 18 – 19 ka (Davies et al., 2020), however, poor age control and lack of geomorphic indicators make it difficult to constrain the ice extent across this region during the deglaciation.

In regards to ice area and extent, our simulated ice sheet at the LGM using TraCE-21ka climate boundary conditions agrees well with the PATICE reconstruction (Figure 10). Our simulations reveal that deglaciation began between 19 ka to 18 ka, consistent with the geologic proxies (Davies et al., 2020). The simulated ice retreat continues until 15 ka, with the largest pulses in ice mass loss occurring at 18.6 ka, 16.8 ka, and 16 ka (Figure 11). Where PATICE estimates an ice cap around 15 ka (~40°S), our simulations reveal that glaciation was restricted to high elevations. After 15 ka, mountain glaciers remain in our simulation but there is no presence of a large ice cap as reconstructed in PATICE. Comparison between the model simulations and PATICE becomes difficult during the 15 -13 ka period as confidence in the geologic reconstruction is low. Therefore, our model results offer a different reconstruction to PATICE, and indicate that the ice sheet in this region largely retreated by 15 ka, with only mountain glaciers remaining. However, during this interval, the Antarctic Cold Reversal (ACR) may have influenced the heat and hydrologic budget across this region, with wetter and cooler conditions interrupting the deglacial warming (Moreno et al., 2018). While TraCE-21ka simulates an ACR, it is short lived, lasting about 500 years as compared to 2,000 years in some ice core records or proxy-based studies (Lowry et al., 2019; He et al., 2013, Pedro et al., 2015). This potential for favorable glacier growth is likely missing in our simulations during the ACR, which may explain some of the mismatch against the PATICE reconstruction at 15 ka – 13 ka.

5 Conclusions

In this study, we use a numerical ice sheet model to simulate the LGM and deglacial ice history across the northernmost extent of the PIS, the CLD. Our LGM ice sheet simulations were driven

https://doi.org/10.5194/tc-2023-68
Preprint. Discussion started: 8 May 2023

by climate model output from five climate models, providing a small ensemble of possible ice sheet states. Additionally, we used transient climate model output covering the last 21 kyr's to simulate the deglaciation of the PIS across the CLD into the early Holocene.

The position, strength, and extent of the SWW played an important role in modulating the size and response of the PIS deglaciation across the CLD. Our simulations indicate that during the LGM, the glacial cooling exerted a large control on the overall size of the PIS across the CLD. However, the simulated LGM precipitation, which varied considerably amongst the climate models, was shown to modulate the ice extent and ice volume across this region. This finding was corroborated by a transient simulation across the last deglaciation where the magnitude of simulated precipitation (in the TraCE-21ka climate model) was modestly higher during the LGM than the preindustrial across the northern portion of the CLD (~10% higher). These results suggest that increases in wintertime LGM and deglacial precipitation have the potential to modulate the timing and magnitude of ice retreat across the CLD. In our case, only modest increases in wintertime precipitation are needed to delay deglaciation up to 2 kyr in our sensitivity tests. Because paleoclimate proxies of past precipitation are often lacking, and climate models simulate a range of possible LGM and deglacial hydrologic states, these results suggest that knowledge of the past precipitation is critical towards better understanding the drivers of PIS growth and demise, especially as small variations in precipitation can modulate ice sheet history on scales consistent with geologic proxies.

Our transient simulation suggests that large scale deglaciation occurs after 19 ka, with the northern portion of the CLD becoming ice free by 17 ka. The PIS persists until 15 ka across the remainder of the CLD, before ice retreats to higher elevation as mountain glaciers and small ice caps (e.g. Cerro Tronador). These results generally agree with the most complete geologic assessment of past PIS history available (PATICE; Davies et al., 2020) for the LGM ice extent and early deglacial, but diverge when considering the ice geometry at and after 15 ka. Because of limited geologic constraints particularly after 15 ka, uncertainty in the timing and extent of deglacial ice history remains. Therefore, our results which illustrate the simulated PIS retreat across the CLD during the last deglaciation may provide insight for future work that aims to improve geologic reconstructions of past ice margin migration.

Code/Data Availability

The simulations performed for this paper made use of the open-source Ice-Sheet and Sea-level System Model (ISSM) and are publicly available at https://issm.jpl.nasa.gov/ (Larour et al., 2012).

Author Contribution

JC, MR, and SM all contributed to the project design. JC performed the model setup and simulations. JC performed the data analysis on model output, with help from MR who performed data analysis on PATICE reconstructions. JC wrote the manuscript with input from MR and SM.

Competing interests

The contact author has declared that none of the authors has any competing interests.

Acknowledgements

https://doi.org/10.5194/tc-2023-68
Preprint. Discussion started: 8 May 2023

The Cryosphere
Discussions

This work was supported by a grant from the National Science Foundation, Frontier Research in Earth Sciences # 2121561.

References

Adhikari, S., Ivins, E. R., and Larour, E., 2016, ISSM-SESAW v1.0: mesh-based computation of gravitationally consistent sea level and geodetic signatures caused by cryosphere and climate driven mass change, Geoscientific Model Development, 9, 9769-9816, doi: 10.5194/gmd-9-1087-2016.

Åkesson, H., Morlighem, M., Nisancioglu, K. H., Svendsen, J. J., and Mangerud, J.: Atmosphere-driven ice sheet mass loss paced by topography: Insights from modelling the south-western Scandinavian Ice Sheet. 2018. Quaternary Sci. Rev., 195, 32–47, https://doi.org/10.1016/j.quascirev.2018.07.004.

Andersen, B., Denton, G. H., & Lowell, T. V. (1999). Glacial geomorphologic maps of Llanquihue drift in the area of the southern Lake District, Chile. Geografiska Annaler: Series A, Physical Geography, 81(2), 155-166.

Bentley, M.J., 1996. The role of lakes in moraine formation, Chilean Lake District. Earth Surf. Process. Landf. 21, 493–507. https://doi.org/10.1002/(SICI)1096-9837(199606)21:6<493::AID-ESP612>3.0.CO;2-D

Bentley, M.J., 1997. Relative and radiocarbon chronology of two former glaciers in the Chilean Lake District. J. Quat. Sci. 12, 25–33. https://doi.org/10.1002/(SICI)1099-1417(199701/02)12:1<25::AID-JQS289>3.0.CO;2-A

Berman, L., Silvestri, G., Tonello, M.S., On differences between Last Glacial Maximum and Mid-Holocene climates in southern South America simulated by PMIP3 models. 2018. Quat. Sci. Rev. 185. 113-121. https://doi.org/10.1016/j.quascirev.2018.02.003.

Blatter, H.: Velocity and stress-fields in grounded glaciers: A simple algorithm for including deviatoric stress gradients. 1995. J. Glaciol., 41, 333-344, https://doi.org/10.3189/S002214300001621X

Boex, J., Fogwill, C., Harrison, S. et al. Rapid thinning of the late Pleistocene Patagonian Ice Sheet followed migration of the Southern Westerlies. 2013. Sci Rep **3**, 2118. https://doi.org/10.1038/srep02118

Boisier, J. P., Alvarez-Garretón, C., Cepeda, J., Osses, A., Vásquez, N., and Rondanelli, R.: CR2MET: A high-resolution precipitation and temperature dataset for hydroclimatic research in Chile. 2018. EGUGA, p. 19739.

Braun, M.H., Malz, P., Sommer, C., Far.as-Barahona, D., Sauter, T., Casassa, G., Soruco, A., Skvarca, P., Seehaus, T.C., 2019. Constraining glacier elevation and mass changes in South America. Nat. Clim. Chang. 9, 130–136. https://doi.org/10.1038/s41558-018-0375-7

Briner, J. P., Cuzzone, J. K., Badgeley, J. A., Young, N. E., Steig, E. J., Morlighem, M., Schlegel, N.-J., Hakim, G., Schaefer, J. Johnson, J. V., Lesnek, A. L., Thomas, E. K., Allan, E., Bennike, O., Cluett, A. A., Csatho, B., de Vernal, A., Downs, J., Larour, E., and Nowicki, S.: Rate of mass loss from the Greenland Ice Sheet will exceed Holocene values this century. 2020. Nature, 6, 70–74, https://doi.org/10.1038/s41586-020-2742-6.

Bondzio, J. H., Seroussi, H., Morlighem, M., Kleiner, T., Rückamp, M., Humbert, A., and Larour, E. Y.: Modelling calving front dynamics using a level-set method: application to Jakobshavn Isbræ, West Greenland. 2016. The Cryosphere, 10, 497–510, https://doi.org/10.5194/tc-10-497-2016

https://doi.org/10.5194/tc-2023-68
Preprint. Discussion started: 8 May 2023

The Cryosphere Discussions

Budd. W.F., P. L. Keage, N. A. Blundy. Empirical studies of ice sliding. 1979. J. Glaciol., 23:157-170.

Caron, L., Ivins, E. R., Larour, E., Adhikari, S., Nilsson, J., and Blewitt, G.: GIA model statistics for GRACE hydrology, cryosphere and ocean science. 2018. Geophys. Res. Lett., 45, 2203–2212, https://doi.org/10.1002/2017GL076644

Choi, Y., Morlighem, M., Rignot, E., and Wood, M.: Ice dynamics will remain a primary driver of Greenland ice sheet mass loss over the next century. 2021. Commun. Earth Environ., 2, 26, https://doi.org/10.1038/s43247-021-00092-z

Cuffey, K. M. and Paterson, W. S. B.: The physics of glaciers, 4th edn. 2010. Butterworth-Heinemann, Oxford, ISBN 9780123694614

Cuzzone, J. K., Schlegel, N.-J., Morlighem, M., Larour, E., Briner, J. P., Seroussi, H., and Caron, L.: The impact of model resolution on the simulated Holocene retreat of the southwestern Greenland ice sheet using the Ice Sheet System Model (ISSM). 2019. The Cryosphere, 13, 879–893, https://doi.org/10.5194/tc-13-879-2019.

Cuzzone, J. K., Young, N. E., Morlighem, M., Briner, J. P., and Schlegel, N.-J.: Simulating the Holocene deglaciation across a marine-terminating portion of southwestern Greenland in response to marine and atmospheric forcings. 2022. The Cryosphere, 16, 2355–2372, https://doi.org/10.5194/tc-16-2355-2022.

Davies, B.J., Darvill, C.M., Lovell, H., Bendle, J.M., Dowdeswell, J.A., Fabel, D., Gheorghiu, D.M., 2020. The evolution of the Patagonian ice sheet from 35 ka to the present day (PATICE). Earth Sci. Rev. 204, 103152. https://doi.org/10.1016/ j.earscirev.2020.103152.

Dias dos Santos, T., Morlighem, M., and Brinkerhoff, D.: A new vertically integrated MOno-Layer Higher-Order (MOLHO) ice flow model. 2022. The Cryosphere, 16, 179–195, https://doi.org/10.5194/tc-16-179-2022.

Fernandez, A., Mark, B.G. 2016. Modeling modern glacier response to climate changes along the Andes Cordillera: A multiscale review, J. Adv. Model. Earth Syst., 8, 467–495, doi:10.1002/2015MS000482.

Garreaud, R., Lopez, P., Minvielle, M., & Rojas, M. (2013). Large-scale control on the Patagonian climate. Journal of Climate, 26(1), 215-230.

GEBCO Bathymetric Compilation Group 2021. 2021. The GEBCO_2021 Grid - a continuous terrain model of the global oceans and land. NERC EDS British Oceanographic Data Centre NOC. doi:10.5285/c6612cbe-50b3-0cff-e053-6c86abc09f8f

Glasser, N. F., Jansson, K. N., Harrison, S., & Kleman, J. (2008). The glacial geomorphology and Pleistocene history of South America between 38 S and 56 S. Quaternary Science Reviews, 27(3-4), 365-390.

Glen, J. W. The creep of polycrystalline ice. 1955. P. Roy. Soc. Lond. A, 228, 519–538, https://doi.org/10.1098/rspa.1955.0066.

Hajima, T., Watanabe, M., Yamamoto, A., Tatebe, H., Noguchi, M. A., Abe, M., Ohgaito, R., Ito, A., Yamazaki, D., Okajima, H., Ito, A., Takata, K., Ogochi, K., Watanabe, S., and Kawamiya, M.: Development of the MIROC-ES2L Earth system model and the evaluation of biogeochemical processes and feedbacks, Geosci. Model Dev., 13, 2197–2244, https://doi.org/10.5194/gmd-13-2197-2020

He, F., Shakun, J. D., Clark, P. U., Carlson, A. E., Liu, Z., Otto-Bliesner, B. L., Kutzbach, J. E. 2013. Northern Hemisphere forcing of Southern Hemisphere climate during the last deglaciation, Nature, 494, 81–85. doi: 10.1038/nature11822.

Heirman, K., De Batist, M., Charlet, F., Moernaut, J., Chapron, E., Brümmer, R., Pino, M., Urrutia, R., 2011. Detailed seismic stratigraphy of Lago Puyehue: implications for the mode and timing of glacier retreat in the Chilean Lake District. J. Quat. Sci. 26, 665–674. https://doi.org/10.1002/jqs.1491

Hinck, S., Gowan, E. J., Zhang, X., and Lohmann, G.: PISM-LakeCC: Implementing an adaptive proglacial lake boundary in an ice sheet model. 2022. The Cryosphere, 16, 941–965, https://doi.org/10.5194/tc-16-941-2022.

Hubbard, A., Hein, A.S., Kaplan, M.R., Hulton, N.R.J., Glasser, N., 2005. A modelling reconstruction of the last glacial maximum ice sheet and its deglaciation in the vicinity of the northern patagonian icefield, south America. Geogr. Ann. Phys.Geogr. 87 (2), 375-391. https://doi.org/10.1111/j.0435-3676.2005.00264.x

Hulton, N.R.J., Purves, R., McCulloch, R., Sugden, D.E., Bentley, M.J., 2002. The last glacial maximum and deglaciation in southern south America. Quat. Sci. Rev. 21 (1), 233-241. https://doi.org/10.1016/S0277-3791(01)00103-2.

Hulton, N., Sugden, D., Payne, A., Clapperton, C., 1994. Glacier modeling and the climate of Patagonia during the last glacial maximum. Quat. Res. 42 (1), 1-19. doi:10.1006/qres.1994.1049

Jiang, N., Yan, Q. Evolution of the meridional shift of the subtropical and subpolar westerly jet over the Southern Hemisphere during the past 21,000 years. 2020. Quat Sci. Rev. 246, https://doi.org/10.1016/j.quascirev.2020.106544.

Kilian, R., Lamy, F., 2012. A review of Glacial and Holocene paleoclimate records from southernmost Patagonia (49e55 S). Quat. Sci. Rev. 53, doi.10.1016/j.quascirev.2012.07.017

Darvill, C.M., Stokes, C.R., Bentley, M.J., Evans, D.J.A., Lovell, H., Dynamics of former ice lobes of the southernmost Patagonian Ice Sheet based on glacial landsystems approach. 2017. J. Quaternary Sci., 32:857-876. https://doi.org/10.1002/jqs.2890

Denton, G.H., Lowell, T.V., Heusser, C.J., Schlüchter, C., Andersen, B.G., Heusser, L.E., Moreno, P.I., Marchant, D.R., 1999. Geomorphology, Stratigraphy, and Radiocarbon Chronology of LlanquihueDrift in the Area of the Southern Lake District, Seno Reloncav., and Isla Grande de Chilo., Chile. Geogr. Ann. Ser. A Phys. Geogr. 81, 167–229. https://doi.org/10.1111/1468-0459.00057

Kohfeld, K.E., Graham, R.M., Boer, A. M. de, Sime, L.C., Wolff, E.W., Qu er e, C.L., Bopp, L., 2013. Southern Hemisphere westerly wind changes during the Last Glacial Maximum: paleo-data synthesis. Quat. Sci. Rev. 68, 76-95. , 10.1016/j.quascirev.2013.01.017

Lamy, F., Kilian, R., Arz, H.W., Francois, J.-P., Kaiser, J., Prange, M., Steinke, T., 2010. Holocene changes in the position and intensity of the southern westerly wind belt.Nat. Geosci. 3, 695–699. https://doi.org/10.1038/ngeo959

Lamy, F., Arz, H. W., Kilian, R., Lange, C. B., Lembke-Jene, L., Wengler, M., ... & Tiedemann, R. (2015). Glacial reduction and millennial-scale variations in Drake Passage throughflow. Proceedings of the National Academy of Sciences, 112(44), 13496-13501 https://doi.org/10.1073/pnas.1509203112

Larour, E., Seroussi, H., Morlighem, M., and Rignot, E.: Continental scale, high order, high spatial resolution, ice sheet modeling using the Ice Sheet System Model (ISSM). 2012. J. Geophys. Res.-Earth, 117, F01022, https://doi.org/10.1029/2011JF002140

https://doi.org/10.5194/tc-2023-68
Preprint. Discussion started: 8 May 2023

Le Morzadec, K., Tarasov, L., Morlighem, M., and Seroussi, H.: A new sub-grid surface mass balance and flux model for continental-scale ice sheet modelling: testing and last glacial cycle. 2015. Geosci. Model Dev., 8, 3199–3213, https://doi.org/10.5194/gmd-8-3199-2015

Leger TPM, Hein AS, Goldberg D,Schimmelpfennig I, Van Wyk de Vries MS, Bingham RG and ASTER Team (2021) Northeastern Patagonian Glacier Advances (43°S) Reflect Northward Migration of the Southern Westerlies Towards the End of the Last Glaciation. Front. Earth Sci. 9:751987. doi: 10.3389/feart.2021.751987

Liu, Z., Otto-Bliesner, B., He, F., Brady, E., Tomas, R., Clark, P., Carlson, A., Lynch-Stieglitz, J., Curry, W., Brook, E., Erickson, D., Jacob, R., Kutzbach, J., and Cheng, J. 2009. Transient simulation of last deglaciation with a new mechanism for Bølling-Allerød warming, Science, 325, 310–314. https://doi.org/10.1126/science.1171041

Lowry, D. P., Golledge, N. R., Menviel, L., and Bertler, N. A. N.: Deglacial evolution of regional Antarctic climate and Southern Ocean conditions in transient climate simulations. 2019. Clim. Past, 15, 189–215, https://doi.org/10.5194/cp-15-189-2019.

Pfeffer, W.T., Arendt, A.A., Bliss, A., Bolch, T., Cogley, J.G., Gardner, A.S., Hagen, J.O., Hock, R., Kaser, G., Kienholz, C. and Miles, E.S. 2014. The Randolph Glacier Inventory: a globally complete inventory of glaciers. Journal of Glaciology, 60, 537-552. Doi:10.31.3189/2014JoG13J176

Lowell, T., Heusser, C., Andersen, B., Moreno, P., Hauser, A., Heusser, L., Schlüchter, C., Marchant, D., Denton, G., 1995. Interhemispheric correlation of late Pleistoceneglacial events. Science 269, 1541–1549. Doi: 10.1126/science.269.5230.1541

Lowry, D. P., Golledge, N. R., Menviel, L., and Bertler, N. A. N.: Deglacial evolution of regional Antarctic climate and Southern Ocean conditions in transient climate simulations. 2019. Clim. Past, 15, 189–215, https://doi.org/10.5194/cp-15-189-2019

Martin J, Davies BJ, Jones R and Thorndycraft V (2022), Modelled sensitivity of Monte San Lorenzo ice cap, Patagonian Andes, to past and present climate. Front. Earth Sci. 10:831631. doi: 10.3389/feart.2022.831631

Mauritsen, T., Bader, J., Becker, T., Behrens, J., Bittner, M., Brokopf, R., Brovkin, V., Claussen, M., Crueger, T., Esch, M., Fast, I., Fiedler, S., Fläschner, D., Gayler, V., Giorgetta, M., Goll, D. S., Haak, H., Hagemann, S., Hedemann, C., Hohenegger, C., Ilyina, T., Jahns, T., Jimenéz-de-la-Cuesta, D., Jungclaus, J., Kleinen, T., Kloster, S., Kracher, D., Kinne, S., Kleberg, D., Lasslop, G., Kornblueh, L., Marotzke, J., Matei, D., Meraner, K., Mikolajewicz, U., Modali, K., Möbis, B., Müller, W. A., Nabel, J. E. M. S., Nam, C. C. W., Notz, D., Nyawira, S.-S., Paulsen, H. Peters, K., Pincus, R., Pohlmann, H. Pongratz, J., Popp, M., Raddatz, T. J., Rast, S., Redler, R., Reick, C. H., Rohrschneider, T., Schemann, V., Schmidt, H., Schnur, R., Schulzweida, U., Six, K. D., Stein, L., Stemmler, I., Stevens, B., von Storch, J.-S., Tian, F., Voigt, A., Vrese, P., Wieners, K.-H., Wilkenskjeld, S., Winkler, A., and Roeckner, E.: Developments in the MPI-M Earth System Model version 1.2 (MPI-ESM1.2) and its response to increasing CO_2, J. Adv. Model. Earth Syst. 2019. 11, 998–1038, https://doi.org/10.1029/2018MS001400

Meier, W.J-H., Grießinger, J., Hochreuther, P., Braun, M.H. 2018. An updated multi-temporal glacier inventory for the Patagonian Andes with changes between the Little Ice Age and 2016. Frontiers in Earth Science, 6, 62. https://doi.org/10.3389/feart.2018.00062

https://doi.org/10.5194/tc-2023-68
Preprint. Discussion started: 8 May 2023

Mercer, J.H., 1972. Chilean glacial chronology 20,000 to 11,000 carbon-14 years ago:some global comparisons. Science 176, 1118–1120. DOI: 10.1126/science.176.4039.1118

Moreno, P. I., Lowell, T. V., Jacobson Jr, G. L., & Denton, G. H. (1999). Abrupt vegetation and climate changes during the last glacial maximumand last termination in the chilean lake district: a case study from canal de la puntilla (41 s). Geografiska Annaler: Series A, Physical Geography, 81(2), 285-311.

Moreno, P.I., Denton, G.H., Moreno, H., Lowell, T.V., Putnam, A.E., Kaplan, M.R., 2015. Radiocarbon chronology of the last glacial maximum and its termination in northwestern Patagonia. Quat. Sci. Rev. 122, 233e249. 10.1016/j.quascirev.2015.05.027

Moreno, P.I., Videla, J., Valero-Garc es, B.L., Alloway, B.V., Heusser, L.E., 2018. A continuous record of vegetation, fire-regime and climatic changes in northwestern Patagonia spanning the last 25,000 years. Quat. Sci. Rev. 198, 10.1016/j.quascirev.2018.08.013

Morlighem, M., Bondzio, J., Seroussi, H., Rignot, E., Larour, E., Humbert, A., and Rebuffi, S.: Modeling of Store Gletscher's calving dynamics, West Greenland, in response to ocean thermal forcing. 2016. Geophys. Res. Lett., 43, 2659–2666, https://doi.org/10.1002/2016GL067695

Muir, R., Eaves, S., Vargo, L., Anderson, B., Mackintosh, A., Sagredo, E., Soteres, R. Late glacial climate evolution in the Patagonian Andes (44-47°S) from alpine glacier modelling. 2023. Quaternary Science Reviews, 305, https://doi.org/10.1016/j.quascirev.2023.108035.

Ohgaito, R., Yamamoto, A., Hajima, T., O'ishi, R., Abe, M., Tatebe, H., Abe-Ouchi, A., and Kawamiya, M.: PMIP4 experiments using MIROC-ES2L Earth system model, Geosci. Model Dev., 14, 1195–1217, https://doi.org/10.5194/gmd-14-1195-2021

Pattyn, F.: A new three-dimensional higher-order thermomechanical ice sheet model: Basic sensitivity, ice stream development, and ice flow across subglacial lakes. 2003. J. Geophys. Res., 108, 2382, https://doi.org/10.1029/2002JB002329

Pedro, J. B., Bostock, H. C., Bitz, C. M., He, F., Vandergoes, M. J., Steig, E. J., Chase, B.M., Krause, C.E., Rasmussen, S.O., Bradley, M.R., Cortese, G. 2016. The spatial extent and dynamics of the Antarctic Cold Reversal. Nature Geoscience, 9(1), 51-55. https://doi.org/10.1038/ngeo2580

Pollard, D. and DeConto, R. M.: Description of a hybrid ice sheet-shelf model, and application to Antarctica. 2012. Geosci. Model Dev., 5, 1273–1295, https://doi.org/10.5194/gmd-5-1273-2012.

Porter, S. C. (1981). Pleistocene glaciation in the southern Lake District of Chile. Quaternary Research, 16(3), 263-292.

Quiquet, A., Dumas, C., Paillard, D., Ramstein, G., Ritz, C., and Roche, D. M.: Deglacial Ice Sheet Instabilities Induced by Proglacial Lakes. 2021. Geophys. Res. Lett., 48, e2020GL092141, https://doi.org/10.1029/2020GL092141

Rojas, M., Moreno, P., Kageyama, M., Crucifix, M, Hewitt, C., Abe-Ouchi, A., Ohgaito, R., Brady, E.C., Hop, P. 2009. The Southern Westerlies during the last glacial maximumin PMIP2 simulations. Clim. Dyn. 32, 525–548. https://doi.org/10.1007/s00382-008-0421-7

Kageyama, M., Harrison, S. P., Kapsch, M.-L., Lofverstrom, M., Lora, J. M., Mikolajewicz, U., Sherriff-Tadano, S., Vadsaria, T., Abe-Ouchi, A., Bouttes, N., Chandan, D., Gregoire, L. J., Ivanovic, R. F., Izumi, K., LeGrande, A. N., Lhardy, F., Lohmann, G., Morozova, P. A., Ohgaito, R., Paul, A., Peltier, W. R., Poulsen, C. J., Quiquet, A., Roche, D. M., Shi, X., Tierney, J. E., Valdes, P. J., Volodin, E., and Zhu, J. 2021. The PMIP4 Last glacial

https://doi.org/10.5194/tc-2023-68
Preprint. Discussion started: 8 May 2023

maximum experiments: preliminary results and comparison with the PMIP3 simulations, Clim. Past, 17, 1065–1089, https://doi.org/10.5194/cp-17-1065-2021.

Tarasov, L. and Peltier, R. W.: Impact of thermomechanical ice sheet coupling on a model of the 100 kyr ice age cycle. 1999. J. Geophys. Res.-Atmos., 104, 9517–9545

Tozer, B., Sandwell, D.T., Smith, W.H.F., Olsen, S.C., Beale, J.R., Wessel, P. Global Bathymetry and Topography at 15 Arc Sec: SRTM15+. 2019. Earth and Space Science. 6, 10, 1847-1864. https://doi.org/10.1029/2019EA000658

Sepulchre, P., Caubel, A., Ladant, J.-B., Bopp, L., Boucher, O., Braconnot, P., Brockmann, P., Cozic, A., Donnadieu, Y., Dufresne, J.-L., Estella-Perez, V., Ethé, C., Fluteau, F., Foujols, M.-A., Gastineau, G., Ghattas, J., Hauglustaine, D., Hourdin, F., Kageyama, M., Khodri, M., Marti, O., Meurdesoif, Y., Mignot, J., Sarr, A.-C., Servonnat, J., Swingedouw, D., Szopa, S., and Tardif, D.: IPSL-CM5A2 – an Earth system model designed for multi-millennial climate simulations, Geosci. Model Dev., 2020. 13, 3011–3053, https://doi.org/10.5194/gmd-13-3011-2020

Sidorenko, D., Goessling, H., Koldunov, N., Scholz, P., Danilov, S., Barbi, D., Cabos, W., Gurses, O., Harig, S., Hinrichs, C., Juricke, S., Lohmann, G., Losch, M., Mu, L., Rackow, T., Rakowsky, N., Sein, D., Semmler, T., Shi, X., Stepanek, C., Streffing, J., Wang, Q., Wekerle, C., Yang, H., and Jung, T.: Evaluation of FESOM2.0 Coupled to ECHAM6.3: Preindustrial and High- ResMIP Simulations, 2019. J. Adv. Model. Earth Sy., 11, 3794–3815, https://doi.org/10.1029/2019MS001696

Sutherland, J. L., Carrivick, J. L., Gandy, N., Shulmeister, J., Quincey, D. J., and Cornford, S. L.: Proglacial Lakes Control Glacier Geometry and Behavior During Recession. 2020. Geophys. Res. Lett., 47, e2020GL088865, https://doi.org/10.1029/2020GL088865

Toggweiler, J.R., Russell, J.L., Carson, S.R. Midlatitude westerlies, atmospheric CO_2, and climate change during the ice ages. 2006. Paleoceanography and Paleoclimatology. 21, https://doi.org/10.1029/2005PA001154

Yan, Q., Wei, T., Zhang, Z. Modeling the climate sensitivity of Patagonian glaciers and their responses to climatic change during the global last glacial maximum. 2022. Quat. Sci. Rev., 288. https://doi.org/10.1016/j.quascirev.2022.107582